
Article:
Benito-Saz, M, Parks, MM, Sigmundsson, F et al. (2017) Repeated magmatic intrusions at El Hierro Island following the 2011–2012 submarine eruption. Journal of Volcanology and Geothermal Research, 344. pp. 79-91. ISSN: 0377-0273

https://doi.org/10.1016/j.jvolgeores.2017.01.020

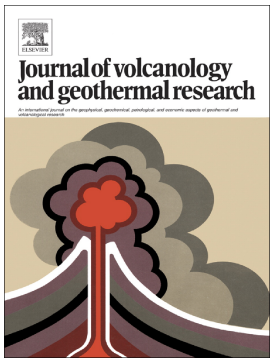

Repeated magmatic intrusions at El Hierro Island following the 2011–2012 submarine eruption

María Á. Benito-Saz, Michelle M. Parks, Freysteinn Sigmundsson, Andrew Hooper, Laura García-Cañada

PII: S0377-0273(17)30071-9
DOI: doi: 10.1016/j.jvolgeores.2017.01.020
Reference: VOLGEO 5999

To appear in: *Journal of Volcanology and Geothermal Research*

Received date: 31 July 2016
Revised date: 10 December 2016
Accepted date: 29 January 2017

Please cite this article as: María Á. Benito-Saz, Michelle M. Parks, Freysteinn Sigmundsson, Andrew Hooper, Laura García-Cañada , Repeated magmatic intrusions at El Hierro Island following the 2011–2012 submarine eruption. The address for the corresponding author was captured as affiliation for all authors. Please check if appropriate. Volgeo(2017), doi: 10.1016/j.jvolgeores.2017.01.020

Repeated magmatic intrusions at El Hierro Island following the 2011-2012 submarine eruption

María Á. Benito-Saz [a*], Michelle M. Parks [b], Freysteinn Sigmundsson [b], Andrew Hooper [c], Laura García-Cañada [a]

[a] Instituto Geográfico Nacional, C/ Alfonso XII, 3, 28014 Madrid, Spain.

[b] Nordic Volcanological Center, Institute of Earth Sciences, University of Iceland, Askja, Sturlugata 7, Reykjavik IS-101, Iceland.

[c] Centre for the Observation and Modelling of Earthquakes and Tectonics (COMET), School of Earth and Environment, University of Leeds, Leeds LS2 9JT, UK.

* Corresponding autor. Tel.: +34 91 792 94 27

E-mail address: mabenito@fomento.es (M.Á. Benito-Saz)

Abstract

After more than 200 years of quiescence, in July 2011 an intense seismic swarm was detected beneath the center of El Hierro Island (Canary Islands), culminating on 10 October 2011 in a submarine eruption, 2 km off the southern coast. Although the eruption officially ended on 5 March 2012, magmatic activity continued in the area. From June 2012 to March 2014, six earthquake swarms, indicative of magmatic intrusions, were detected underneath the island. We have studied these post-eruption intrusive events using GPS and InSAR techniques to characterize the ground surface deformation produced by each of these intrusions, and to determine the optimal source parameters (geometry, location, depth, volume change). Source inversions provide insight into the depth of the intrusions (~11-16 km) and the volume change associated with each of them (between 0.02 and 0.13 km^3). During this period, more than 20 cm of uplift was detected in the central-western part of the island, corresponding to approximately 0.32-0.38 km^3 of magma intruded beneath the volcano. We suggest that these intrusions result from deep magma migrating from the mantle, trapped at the mantle/lower crust discontinuity in the form of sill-like bodies. This study using joint inversion of GPS and InSAR data in a post-eruption period provides important insight into the characteristics of the magmatic plumbing system of El Hierro, an oceanic intraplate volcanic island.

1. Introduction

Ground deformation may occur at active volcanoes due to a variety of magmatic and non-magmatic processes, e.g. migration of magma, gas exsolution, slope instabilities, etc. (Battaglia et al., 2006; Nishimura et al., 2001; Sigmundsson et al., 2010; Solaro et al., 2010; Watson et al., 2000). This study focuses on ground deformation measured at El Hierro Island, Spain, between June 2012 and March 2014, and deformation modeling that suggests magmatic processes are responsible for the observed deformation during this period. In general, injection of batches of magma rising from the mantle to shallower levels in the crust can produce detectable surface inflation. For example, a magmatic intrusion between July 2007 and July 2008 beneath the Okmok caldera in the Aleutian Islands, Alaska, produced 15 cm of uplift shortly before the 12 July 2008 eruption (Lu et al., 2010), and between 2007 and 2009, 13 cm of uplift was detected in Slamet volcano, Java Island, a short time before the April 2009 eruption (Chaussard and Amelung, 2012). These magmatic intrusions are usually tracked by changes in seismicity and geodetic observations. However, they do not always lead to an eruption. Paka volcano, East African Rift, displayed approximately 21 cm of uplift during 2006-2007 without any subsequent eruption (Biggs et al., 2009). In Iceland, a series of shallow sills were intruded beneath Eyjafjallajökull volcano in 1994 and 1999, but an eruption did not occur until 2010 (Sigmundsson et al., 2010).

Although numerous studies have been undertaken describing magmatic intrusions and their associated surface deformation, observations at oceanic intraplate volcanic islands are limited. These kinds of islands (Canary Islands, Hawaii, Galapagos, Reunion, Cape Verde, etc.) are often highly populated and a tourist destination for thousands of people so even a small eruption can have a major economic and social impact. Understanding the characteristics of these magmatic intrusions is essential for

obtaining an improved understanding of the likely volcanic hazards in the event of an eruption.

A magmatic intrusion in El Hierro Island (Canary Islands, Spain) was detected in the center of the island on 19 July 2011 at a depth of 9-11 km after more than 200 years of quiescence. The intrusion produced more than 5 cm of surface deformation and almost 10000 earthquakes, migrating 15 km laterally until a submarine eruption commenced on 10 Oct 2011, 2 km off the southern coast (Domínguez Cerdeña et al., 2014; López et al., 2012; Rivera et al., 2013). The eruption lasted almost five months and produced discolored water, large gas bubbles, lava fragments and pyroclasts on the sea surface (Carracedo et al., 2012; López et al., 2014; Martí et al., 2013b). However, the end of the submarine eruption did not mark the end of the magmatic activity at this young oceanic island. At least six additional intrusions have been revealed by seismicity and ground deformation observations during the period spanning June 2012 to March 2014 (Klügel et al., 2015).

The aim of this study is to jointly analyze Interferometric Synthetic Aperture Radar (InSAR) and Global Positioning System (GPS) measurements to quantify the ground deformation produced by each of these six post-eruption intrusive events at El Hierro. These geodetic datasets have been inverted to determine the optimal source parameters (location, geometry and volume/pressure change) that best define these intrusions from a geodetic and volcanological point of view. Results have been interpreted with the aid of seismicity for each period of unrest to gain an improved understanding of the geodetic signals and the characteristics of these magmatic intrusions.

2. El Hierro Island

2.1. Geological Setting

The archipelago of the Canary Islands is a group of seven main volcanic islands near the northwest coast of Africa with historical Hawaiian and Strombolian volcanic activity (Romero Ruíz, 1990). The smallest and youngest within this group of intraplate islands, El Hierro is a young volcanic edifice within its main shield-building stage, with the oldest subaerial rocks dated at 1.12 Ma (Guillou et al., 1996). El Hierro rises from around 3800 m below sea level to a maximum altitude of 1502 m at its most central part, having a subaerial surface of 269 km^2. More than 200 submarine cones have been identified, providing El Hierro with the highest density of recent, well-preserved craters compared to the remaining islands of the archipelago (Guillou et al., 1996; Rivera et al., 2013) (Fig. 1).

The abrupt topography of the island is the result of the formation of different basaltic edifices and the occurrence of several large lateral landslides. El Tiñor volcano, developed in the north-eastern part of the island between 1.12 and 0.88 Ma ago, later experienced a northwest flank collapse. Following this, El Golfo edifice began forming around 545 ka ago, overlying the El Tiñor volcano on its west flank and completely filling the El Tiñor collapse (Carracedo et al., 1999; Guillou et al., 1996). Subsequently, several lateral collapses modified this edifice. The El Julan landslide, >200 ka ago, destroyed the southwest flank of the edifice when it was probably already well-developed, forming a 10-km-wide embayment. In addition, Las Playas collapses formed a 4-km-wide embayment and a 1000-m high cliff, destroying the southeast flank of the edifice around 176-145 ka (Gee et al., 2001b). The collapse of the northern flank during the El Golfo landslide has been identified as the youngest large-scale landslide in the Canary Islands, ~87-39 ka (Carracedo et al., 1999; Gee et al., 2001b; Longpré et al.,

2011; Masson, 1996; Masson et al., 2002; Urgeles et al., 1997). The embayment formed is almost 14-km-wide and presents a vertical escarpment of around 1400-m-high, a distinctive landmark on the island (Fig. 1).

Over the last 145 ka, volcanism has been monogenetic, characterized by the eruption of mafic magmas forming cinder cones and lava flows (Carracedo et al., 2001; Stroncik et al., 2009). These eruptive centers have been concentrated along three rifts, built on top of the remains of the previous edifices, which extend from the center of the island (Carracedo, 1994; Carracedo et al., 2001; Guillou et al., 1996) (Fig. 1). These rifts are characterized by submarine elongations reflected both in bathymetry and aeromagnetic data (Acosta et al., 2003; Blanco-Montenegro et al., 2008; Gee et al., 2001a; Münn et al., 2006). However, the idea of a three-armed rift system has been debated since volcanic activity has not been confined to narrow zones (Gee et al., 2001a), and the structural elements on the entire volcanic edifice (subaerial and submarine) display a radial strike distribution with respect to the center of the island (Becerril et al., 2015).

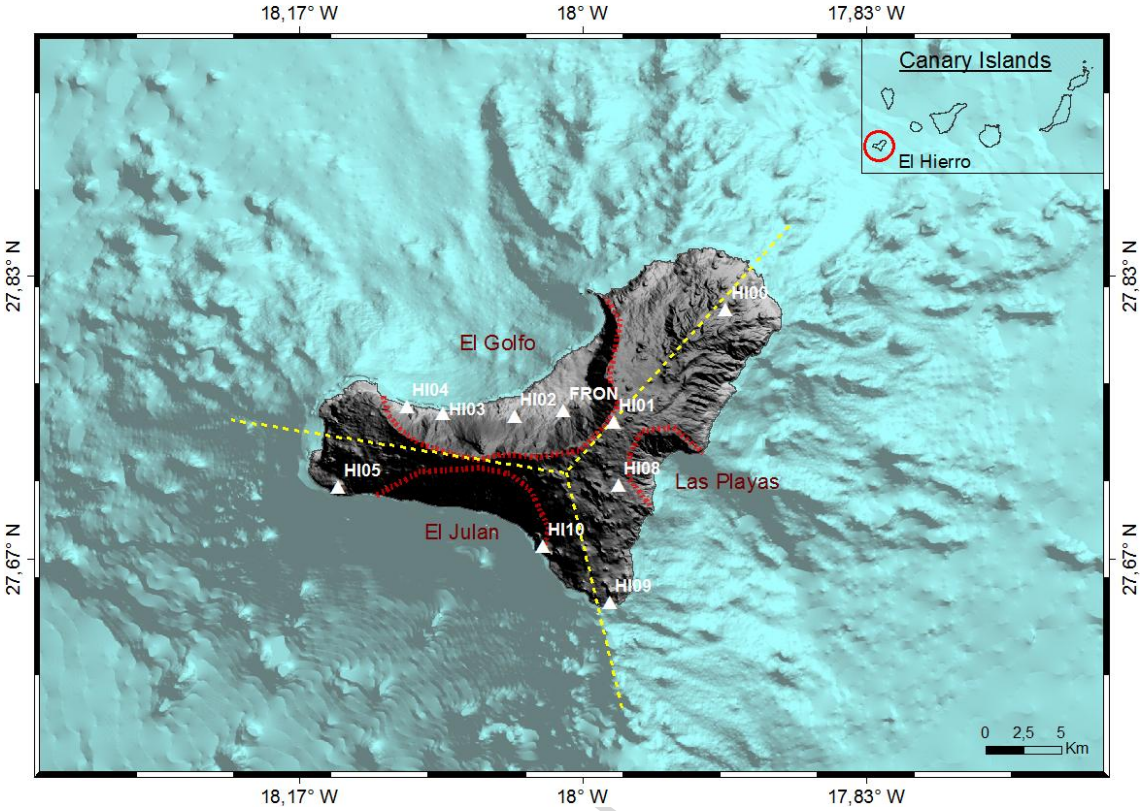

Fig. 1. Shaded relief map of topography and bathymetry of El Hierro Island. The inset in the top right of the figure shows the location of El Hierro Island in the Canary archipelago. Yellow dashed lines display the traces of the three-armed rifts (spaced about 120º) oriented in northeast, northwest and south directions (Carracedo et al., 2001); red dashed lines indicate the approximate location of the lateral landslides that formed the embayments of El Golfo, El Julan, and Las Playas. Continuous GPS (cGPS) stations used in this study are represented by white triangles.

2.2. Volcanic Activity

2.2.1. Previous activity

Historical records in El Hierro Island span approximately the last 600 years and during this time, no documentation or samples have been found to verify the occurrence of a volcanic eruption on the island prior to the 2011-2012 submarine eruption. A seismic crisis in 1793 is well documented in historic chronicles (Darias y Padrón, 1929) but no evidence exists to substantiate a volcanic eruption during this period (Villasante-Marcos and Pavon-Carrasco, 2014). Seismic activity over the last two decades has remained low, with less than six detected earthquakes per year.

2.2.2. The 2011 pre-eruptive unrest at El Hierro

On 19 July 2011, an intense seismic swarm began at El Hierro Island (Carracedo et al., 2012; Ibáñez et al., 2012; López et al., 2012; Martí et al., 2013b). Initial seismic activity of low magnitude (<M2.6) started in the central part of the island and migrated 3 km towards north at depths of 9-11 km over a period of one month (Domínguez Cerdeña et al., 2014). From the beginning of September to the beginning of October 2011, seismicity migrated approximately 15 km southward and both the earthquakes magnitude and the rate of ground deformation increased (González et al., 2013; López et al., 2012). A 45 μGal gravity decrease was recorded at two gravimeters installed in the island associated with the lateral migration of the magma (Sainz-Maza Aparicio et al., 2014). In addition, anomalous levels of radon, CO_2 emissions, helium emissions from the soil, and 3He/4He ratios in groundwater were also recorded (López et al., 2012; Melián et al., 2014; Padilla et al., 2013; Padron et al., 2013; Pérez et al., 2012). During the first days of October 2011, seismicity spread to the southeast, approaching the south coast of the island, located at depths of 12-14 km and releasing more than

50% of the total seismic energy documented for the whole unrest period. At least 90 felt earthquakes were reported by the population and a five day-long cycle of deflation/re-inflation was observed (Domínguez Cerdeña et al., 2014; López et al., 2012; Martí et al., 2013b). On 8 October 2011, the largest earthquake of the unrest swarm, a Mw 4.0 event, occurred at a focal depth of 12-13 km (del Fresno et al., 2015). This was followed swiftly by the onset of a swarm of low magnitude, shallow earthquakes (>80 events in 30 hours, with depths ≤4 km and magnitudes <M2.5) clustered at a distance of ~13 km south from the previous site of activity (López et al., 2014) (Fig. 2a).

2.2.3. The 2011-2012 submarine eruption of El Hierro

On 10 October 2011, a volcanic eruption started at El Hierro Island, identified by a clear harmonic tremor signal on seismic records. At the same time, dead fish were seen floating on the sea surface 2 km off the southern coast, ~4 km north of where the previous shallow earthquakes were detected. Tremor amplitude continually increased until 12 October 2011 when this abruptly ceased and green-colored water and the first rock samples were observed floating on the sea (López et al., 2014). These rocks were called xenopumices due to their glassy basanitic crusts of decimeter-scale and cores of pumice-like texture and glassy matrix (Del Moro et al., 2015; Meletlidis et al., 2012; Sigmarsson et al., 2013; Troll et al., 2012).

During the first days of the eruption, low magnitude seismic events (<M3) occurred in the area of previous seismicity. From mid-October, seismicity occurred in the northern and central part of the island at two different levels with depths located between 20-25 km and 15-20 km respectively (Fig. 2b). Strong bubbling was observed on the sea surface accompanied with ash and scoriaceous fragments. Slight deflation was measured on the GPS stations installed on the island (Martí et al., 2013b; Meletlidis

et al., 2015). From the end of October until 23 February 2012, lava balloons, up to two meters long consisting of a gas-filled cavity surrounded by a few centimeters-thick crust of basanite lava, were observed on the sea surface (Longpré et al., 2014; Martí et al., 2013a). From January to March 2012 volcanic tremor signal progressively weakened and no significant ground deformation was detected. During this period, seismic activity returned to the central and southern part of the island (Meletlidis et al., 2015) (Fig. 2b).

The eruption officially ended on 5 March 2012. A new volcanic cone was formed with its summit located at a depth of 89 m below sea level. The non-dense rock equivalent volume of this cone was 329×10^6 m^3 (i.e., volume of the volcanic material accumulated without porosity corrections) (Rivera et al., 2013). This submarine eruption has been the first eruption of the 21st century in the Canary Islands, the first historical eruption recorded at El Hierro Island, and the first eruption and associated unrest to be fully monitored in real time in the Canaries archipelago.

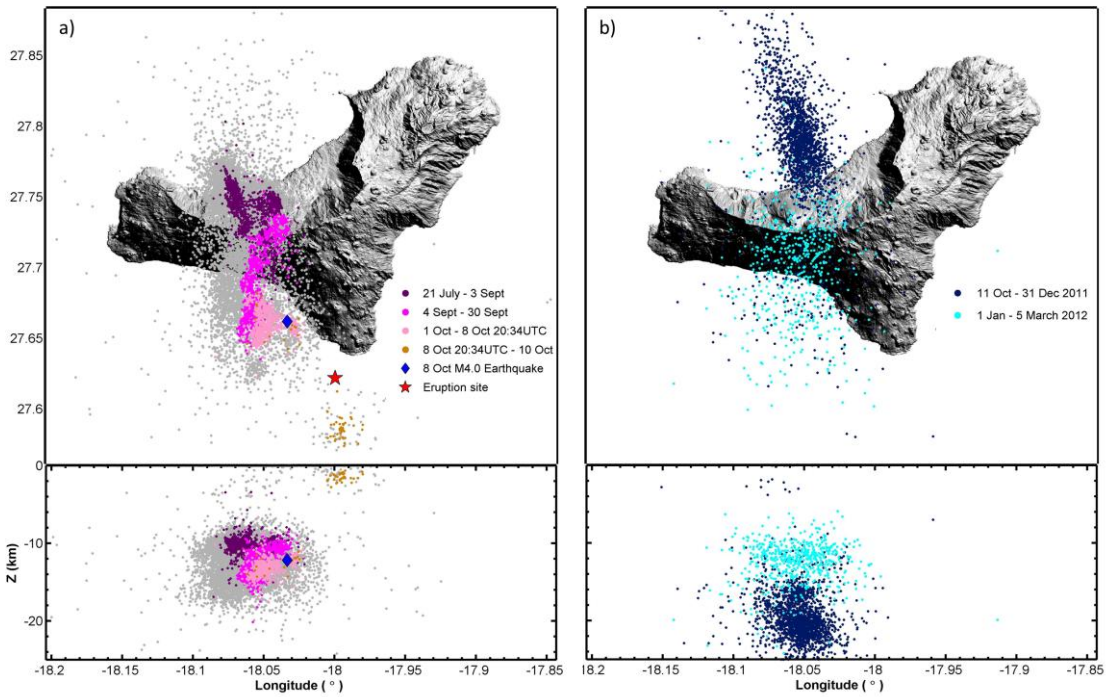

Fig. 2. Temporal evolution of seismicity, throughout the unrest and eruptive periods at El Hierro Island. a) Relocated earthquakes in color and non-relocated events in grey for the 2011 unrest period, 21 July 2011 - 10 October 2011 (Dominguez Cerdeña et al., 2014; IGN seismic catalog, www.ign.es). Blue diamond represents the Mw 4.0 seismic event on 8 October 2011 (del Fresno et al., 2015). Red star indicates the 2011 eruption site (Rivera et al., 2013). b) Seismic events (not relocated) for the eruption period, 11 October 2011 - 5 March 2012 (IGN seismic catalog). Bottom panels show the depth of the earthquakes in east-west direction.

2.2.4. The 2012-2014 magmatic intrusions at El Hierro

The end of the 2011-2012 submarine eruption did not mark the end of this phase of magmatic activity at El Hierro. At least six post-eruption episodes, each of them characterized by an intense seismic swarm and rapid elevated rates of deformation, have been detected on the island from June 2012 to March 2014 (Díaz-Moreno et al., 2015; García et al., 2014; González et al., 2013; Klügel et al., 2015; Meletlidis et al., 2015; Telesca et al., 2016). Based on the observed uplift and seismic activity, these episodes have been interpreted as intrusions of magma in the region of the uppermost mantle or the lower oceanic crust (Díaz-Moreno et al., 2015; Klügel et al., 2015) (Fig. 3). Since March 2014, no significant ground deformation has been detected on the island and remnant seismic activity has occurred at a rate of ~15 earthquakes per month.

This study focusses on characterizing the ground surface deformation at El Hierro Island produced by each of these 2012-2014 post-eruption magmatic intrusions, and determining the most likely deformation sources with the goal of better understanding the magmatic plumbing system beneath El Hierro.

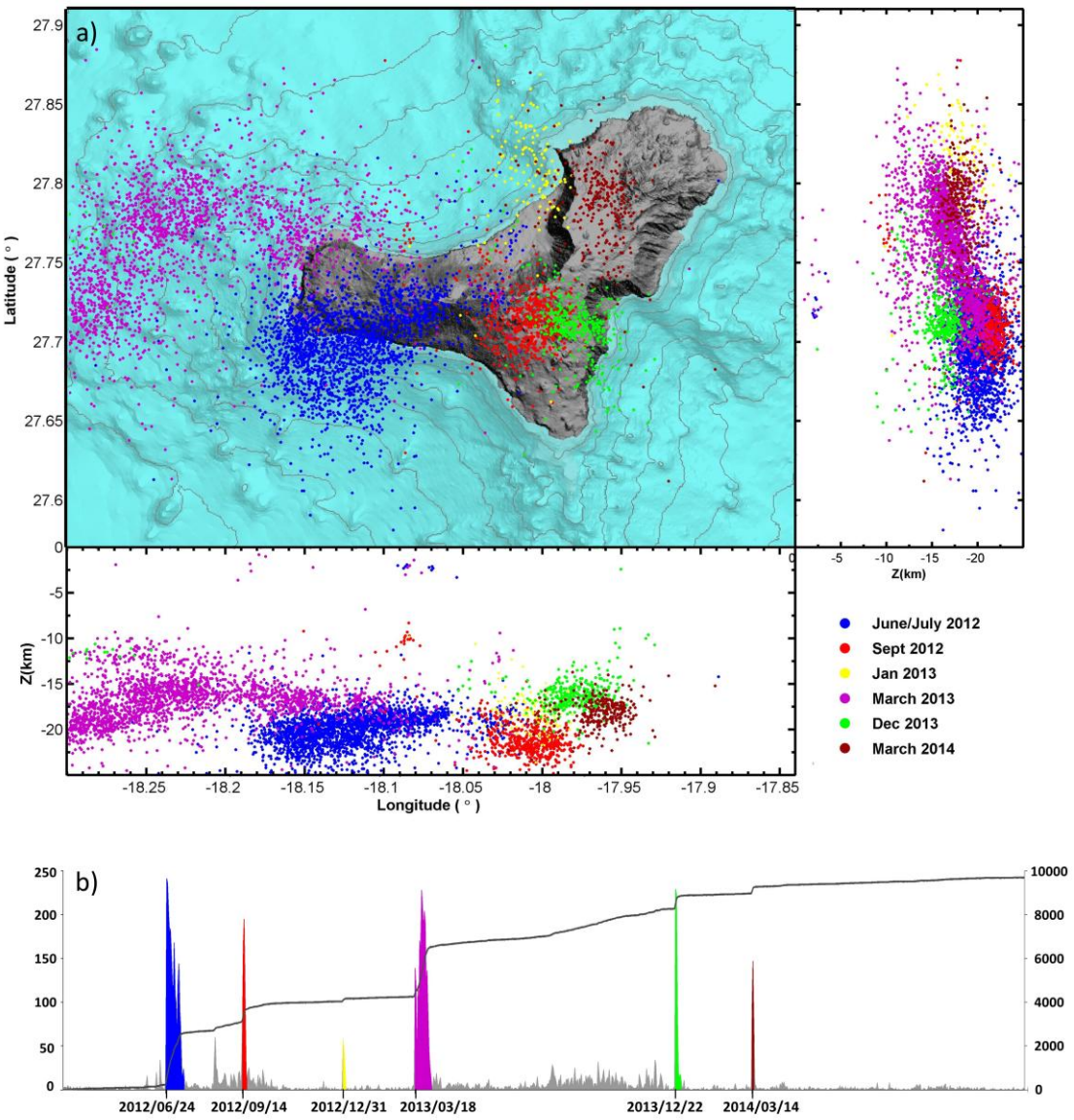

Fig. 3. a) Location of seismicity for each of the 2012-2014 post-eruption magmatic intrusive events at El Hierro Island (IGN seismic catalog). Vertical cross sections in north–south direction (right panel) and east–west direction (bottom panel) show the depth of the earthquakes. b) Daily number of earthquakes (left scale) (in grey, inter-intrusive activity; in color, magmatic intrusions) and cumulative number of earthquakes (right scale) from March 2012 to December 2014.

3. Methods

3.1. GPS

A network of ten continuous GPS (cGPS) stations was operating at El Hierro from June 2012 to March 2014 (Fig. 1). All the stations showed significant deformation related to the El Hierro post-eruption magmatic intrusions. cGPS station FRON was maintained by the Canarian Regional Government (GRAFCAN). cGPS station HI00 was owned by the University of Cádiz (UCA) whereas the remainder of the cGPS stations were operated by the National Geographic Institute of Spain (IGN). The GPS data (30-second sampling) were analyzed using Bernese software version 5.2 (Dach et al., 2015) in the framework of a regional GPS network consisting of more than 30 GPS stations located in the Canary Islands and surrounding areas (Azores, south of Spain and north of Africa). The data were processed in the ITRF2008 reference frame and station coordinates determined using minimum constraints to an International GNSS Service (IGS) core site group of five stations. Ocean-loading model FES2004, IGS absolute antenna phase center models, and precise satellite orbits were applied. Daily north, east, and vertical deformation components and their associated errors were calculated and utilized in the deformation modeling.

3.2. InSAR

InSAR is a well-established geodetic technique that has been extensively used to measure and monitor ground deformation in volcanic areas for several decades (Dzurisin et al., 2006; Hooper et al., 2012; Massonnet et al., 1993; Pinel et al., 2014; Pritchard and Simons, 2004; Wicks et al., 2002). The main advantages of InSAR over other conventional geodetic techniques are its spatial coverage, the unmanned day or night data collection, and the possibility to measure deformation over timescales

spanning days to decades using stored images. Active radar satellites illuminate a swath of the Earth's surface with electromagnetic radiation in the microwave frequency band and record the backscattered waves. If the ground surface deforms between two passes of the satellite over the same area, the displacement can be measured by observing the difference in the phase between the two radar returns in the satellite's the line-of-sight (LOS). The resulting interferometric phase is the combination of differences in orbital position, topography, atmospheric delays and ground deformation. To separate out the phase change resulting from deformation only, the other components must first be removed (Massonnet and Feigl, 1995; Massonnet and Feigl, 1998; Zebker et al., 1994). As the interferometric phase has values between 0 and 2π, to obtain the ground deformation in metric units, a phase unwrapping process is applied, adding the correct multiple of 2π to the InSAR phase (Goldstein et al., 1988).

Interferometric analysis of 24 single look complex (SLC) images from the Canadian RADARSAT-2 (RDS-2) satellite (C-band, 5.6 cm wavelength) and 20 SLC scenes from the Italian COSMO-SkyMed (CSK) satellites (X-band, 3.1 cm wavelength) was undertaken to measure the surface deformation related to each of the six post-eruption intrusive episodes in El Hierro Island spanning the period June 2012-March 2014. Satellite scenes were chosen, when possible, with minimum cloud coverage at the time of satellite acquisition, using for this purpose meteorological satellite images (since we had limited quota for satellite images). The data fully covers each of the intrusive episodes in both ascending and descending passes (Supplementary Table 1).

Interferograms were processed using the Stanford Method for Persistent Scatterers software, StaMPS (Hooper, 2008; Hooper et al., 2007; Hooper et al., 2004). This code utilizes the DORIS software package (Kampes et al., 2003) to create the interferograms and is unwrapped using a 3-D statistical-cost phase-unwrapping

algorithm (Hooper, 2010). A 5 m resolution digital elevation model (DEM) of El Hierro Island (provided by the Spanish IGN) was used to remove the topographic contribution to the interferometric phase. We employed time-series analyses in order to reduce random atmospheric noise, orbital inaccuracies, phase unwrapping and DEM errors. StaMPS includes Persistent Scatterer (PS) and Small Baseline (SB) time-series approaches for time-series generation. We combined both methods, increasing the extraction of signal from more pixels than either method alone.

Often highly vegetated areas and steep slopes produce areas of decorrelation, and local atmospheric effects are usually difficult to eliminate without removing part of the deformation signal (Bekaert et al., 2015b). This is particularly notorious in the case of oceanic islands and, especially, in the case of El Hierro, where the steep relief of the island introduces variations in the interferometric phase due to temporal changes in temperature, pressure and water vapor (Gonzalez et al., 2010; González et al., 2013; Parks et al., 2011). Previous InSAR analyses carried out in El Hierro Island indicate that the observed atmospheric signal is largely correlated with topography (Bekaert et al., 2015b). Taking this into account, we applied a linear phase-based method, extracting the topographically correlated phase using the Toolbox for Reducing Atmospheric InSAR Noise (TRAIN) (Bekaert et al., 2015a) (Supplementary Figs. 1-5). Wrapped interferograms are presented in Supplementary Fig. 6.

3.3. Modeling

A joint inversion of the GPS and InSAR data sets was carried out to determine the approximate volcanic source (location, depth, geometry and volume change (ΔV)) responsible for the observed ground deformation during each of the 2012-2014 post-eruption intrusive episodes. We tested a spherical point pressure source (Mogi, 1958), a spheroid source (Yang et al., 1988), a horizontal penny-shaped crack representing a circular sill-like source (Fialko et al., 2001), and a rectangular dislocation representing an opening dike (Okada, 1985; Okada, 1992). Position of the source, ΔV, radius of the penny-shaped crack and spheroid, opening of the dyke as well as strike and dip of the dyke and spheroid were all free parameters. An elastic homogeneous, isotropic, half-space was assumed with Poisson's ratio of 0.25, shear modulus of 40 GPa (Watts, 1994; Watts et al., 1997), and a traction-free surface. We applied a Markov chain Monte Carlo (MCMC) sampling algorithm incorporating the Metropolis algorithm to calculate the posterior probability distribution and the confidence intervals of all our model parameters, assuming a uniform prior probability (Hooper et al., 2007; Mosegaard and Tarantola, 1995; Sigmundsson et al., 2015).

For the input to the modeling, we selected the interferograms that covered each of the entire intrusive periods containing the minimum atmospheric component (Table 1; Supplementary Fig. 7). We down-sampled all interferograms using an adaptive quad-tree approach (Decriem et al., 2010), reducing the computational time while preserving the deformation pattern (Supplementary Fig. 8). The error covariance matrix for the interferograms was calculated from modelled semi-variograms assuming a one-dimensional exponential covariance function and using interferograms between intrusive events that did not show any ground deformation (Supplementary Fig. 9). GPS uncertainties estimated during the Bernese processing were used in the GPS error

covariance matrix to determine the weight of the GPS data in the inversions. During the modeling, the elevation of the geodetic stations was not taken into consideration. Therefore, depths obtained here are referenced to a surface approximately equal to the average observation height, ~420 m. Measurement errors were calculated assuming a zero-mean normal distribution.

This method enabled us to jointly invert the three components of the GPS observations (north, east, up) together with InSAR data (displacements in the LOS direction) from multiple satellites working with different frequencies bands and acquisition geometries.

The different models applied were assessed by calculating the weighted residual sum of squares, RSS:

$$RSS=r^{T}\Sigma^{-1}r \quad (1)$$

where r is the residual vector, difference between the observed and the predicted data, and Σ^{-1} is the inverse of the data error covariance matrix) normalized by the degrees of freedom (number of data points minus number of free model parameters: 4 model parameters for the sphere point pressure source, 5 for the penny-shaped crack, 7 for the spheroid, and 8 for the Okada rectangular dislocation). The best fit model was inferred from the lowest RSS value.

Observed, modeled, and residual interferograms, along with GPS displacements, for the best-fitting sources (sphere, spheroid, penny-shaped crack and rectangular dislocation) (Table 2; Supplementary Fig. 10) are shown in Supplementary Figs. 11-25. Model parameter uncertainties are presented as a posteriori probability density functions in Supplementary Figs. 26-31.

Table 1. Interferograms used in the modeling. Bp is the perpendicular baseline, distance between the two satellite acquisition positions perpendicular to the line-of-sight.

	Satellite	Dates (yyyy/mm/dd)	Sensor mode	Path	B_p (m)	Time interval (days)	Heading (°)	Look angle (°)
2012 June/July intrusion	RSAT2	2012/04/28 – 2012/08/02	Standard 6	Ascending	203	96	347.01	36.62
	RSAT2	2012/02/09 – 2012/08/19	Standard 7	Ascending	-6	192	347.00	40.50
	CSK	2012/06/10 – 2012/09/01	TR_HIMAGE	Ascending	616	83	348.28	29.37
	CSK	2012/02/21 – 2012/07/30	STR_HIMAGE	Descending	617	160	192.69	34.66
2012 September intrusion	CSK	2012/09/01 – 2012/12/22	STR_HIMAGE	Ascending	-215	112	348.28	29.37
	CSK	2012/07/30 – 2012/09/24	STR_HIMAGE	Descending	352	56	192.69	34.66
2013 January intrusion	CSK	2012/12/22 – 2013/01/11	STR_HIMAGE	Ascending	905	20	348.28	29.37
	CSK	2012/09/24 – 2013/01/06	STR_HIMAGE	Descending	-480	104	192.69	34.66
2013 March/ April intrusion	RSAT2	2013/03/06 – 2013/04/23	Standard 6	Ascending	385	48	347.01	36.62
	CSK	2013/01/11 – 2013/04/26	STR_HIMAGE	Ascending	-1576	105	348.28	29.37
	CSK	2013/01/06 – 2013/05/07	STR_HIMAGE	Descending	-1048	121	192.69	34.66
2013 December intrusion	CSK	2013/12/13 – 2014/02/27	STR_HIMAGE	Ascending	76	3	348.28	29.37
	CSK	2013/12/17 – 2014/01/05	STR_HIMAGE	Descending	817	19	192.69	34.66
2014 March intrusion	CSK	2014/02/27 – 2014/04/04	STR_HIMAGE	Ascending	323	56	348.28	29.37
	CSK	2014/01/05 – 2014/03/30	STR_HIMAGE	Descending	1219	84	192.69	34.66

4. Results

4.1. 2012 June/July intrusion

Four months after the end of the submarine eruption, an intense seismic swarm was detected in the center of the island on 24 June 2012. Seismicity clearly migrated southwest for approximately 15 km over a period of 20 days. More than 2000 earthquakes were located during this time, with daily maximum magnitudes above M3, and at least 4 earthquakes with magnitudes above M4 occurring on 27 June, and 2, 3 and 10 of July. All cGPS stations showed elevated rates of horizontal and vertical deformation. More than 9 cm of horizontal deformation and 9.5 cm of vertical deformation was registered at cGPS station HI05. Unwrapped interferograms show a clear uplift in the central-western part of the island both in ascending and descending passes (Fig. 4.1).

Modeling of the volcanic source responsible for such ground deformation during the entire intrusive episode shows that the deformation data favor a spheroid source (minimum RSS value, 1.47) with a volume change (ΔV) of 0.092±0.006 km^3 located south of the epicenters and at a depth of ~10 km (Table 2; Supplementary Figs. 10-14, 26).

4.2. 2012 September intrusion

Two months after the end of the June-July 2012 intrusion, another intense seismic swarm was detected on 14 September 2012. This new seismic activity was confined to the center of the island and lasted only five days. However, more than 500 earthquakes were located during this time (with maximum magnitudes above M3) and all cGPS stations showed clear deformation (4 cm of vertical deformation was registered at cGPS station HI09 and more than 2 cm of horizontal deformation at cGPS

station HI01). Unwrapped interferograms indicate that most of the deformation occurred in the southern part of the island (Fig. 4.2).

Joint inversion of GPS and InSAR data suggest a source in the southern part of the island at ~11-16 km depth corresponding to a volume change of 0.022-0.030 km^3. The best fit model (RSS=1.41) is a prolate spheroid at ~12 km depth with a volume change of 0.027±0.002 km^3 whereas the horizontal penny-shaped crack representing a sill-like source (RSS=1.55) is the deepest model, located at a depth of ~16 km (base of seismicity), with a radius of ~1.7 km and ΔV of 0.030±0.008 km^3 (Table 2; Supplementary Figs. 10, 15-16, 27).

4.3. 2013 January intrusion

During the end of 2012 and beginning of 2013, more than 100 earthquakes were located in the northeastern part of the island for four days. The maximum magnitude registered was M2.6. All cGPS stations showed clear horizontal and vertical motion (almost 2 cm of horizontal deformation at cGPS station HI00 and more than 3.5 cm of vertical deformation at cGPS station FRON). Unwrapped interferograms show how most of the displacement is confined to the northern part of the island (Fig. 4.3).

All models obtained from the joint inversion of GPS and InSAR data show similar RSS (1.40-1.43) and are located in the central-northern part of the island. The deepest model source is sill-like at ~16 km depth, whereas the point pressure source and the spheroid models are located at ~12 km depth. The volume change for these models ranges from 0.023 to 0.028 km^3 (Table 2; Supplementary Figs. 10, 17-18, 28).

4.4. 2013 March/April intrusion

The second longest post-eruption intrusive event commenced on 18 March 2013 and lasted for approximately 18 days. Seismicity started in the northwestern part of the island and clearly migrated to the west for almost 30 km. All cGPS stations showed eastward and upward displacements, with the maximum displacements recorded at the most western station of the island, cGPS station HI05, detecting more than 9 cm of eastward displacement and almost 12 cm of vertical displacement. Unwrapped interferograms show the largest deformation occurs in the western part of the island (Fig. 5.1). More than 2000 earthquakes were located during this period. Earthquakes with magnitude >M4 were registered between 25 and 31 March 2013, with the largest earthquake (M4.9) occurring on 31 March.

Although the inversion of the GPS and InSAR data for the entire period of time show that the optimal model is an Okada dislocation (RSS=0.96), the location of earthquake hypocenters suggests the best fit models are either a sphere or spheroid located at the base of the seismicity, ~11 km depth, with ΔV of 0.124-0.133 km^3, (RSS=1.05-1.04), respectively (Table 2; Supplementary Figs. 10, 19-21, 29).

4.5. 2013 December intrusion

More than eight months after the January 2013 intrusion, an intense seismic swarm was detected on 22 December 2013 and lasted approximately six days. More than 500 earthquakes were recorded in the central-eastern part of the island. An earthquake of M5.1 was detected on 27 December 2013. cGPS station HI10 recorded 4.1 cm of horizontal deformation and 8 cm of vertical deformation. The area exhibiting the largest deformation occurs in the south of the island as shown by the unwrapped interferograms (Fig. 5.2).

The optimal source model obtained from the joint inversion of GPS and InSAR data is a spheroid located south of the earthquakes at a depth of ~11 km with a volume change of 0.041±0.005 km^3. The sill-like source is deeper, located at ~14 km depth, with a radius of ~1.6 km and a volume change of 0.044±0.013 km^3 (Table 2; Supplementary Figs. 10, 22-23, 30).

4.6. 2014 March intrusion

The last and shortest intrusive event occurred from 14 to 16 March 2013. Almost 300 earthquakes were located during these three days in the northeastern part of the island with maximum magnitudes <M2.5. cGPS station HI00 registered 1.4 cm of horizontal deformation and 3.7 cm vertical deformation. Unwrapped interferograms indicate that most of the ground surface displacement is confined to the area of seismicity (Fig. 5.3).

All the models obtained from the joint inversion of GPS and InSAR observations present a similar fit to the data (RSS=0.62-0.63). The sphere and the prolate spheroid are located at ~12-13 km depth whereas the rectangular dislocation and the penny-shaped crack model, both representing a sill-like source, are located at ~15-16 km depth. The associated volume change is between 0.023-0.028 km^3 (Table 2; Supplementary Figs. 10, 24-25, 31).

Fig. 6 shows the optimal location of the spheroid and penny-shaped crack deformation sources, determined through joint inversion of GPS and InSAR data for each post-eruption intrusive event. For the entire time period spanning June 2012 to March 2014, GPS measurements display more than 27 cm of vertical displacement at cGPS station HI10, more than 10 cm of eastward displacement at cGPS station HI01

and more than 13 cm of northward displacement at cGPS station HI04. Unwrapped interferograms indicate that the majority of the deformation occurred in the central-western part of the island (Fig. 7).

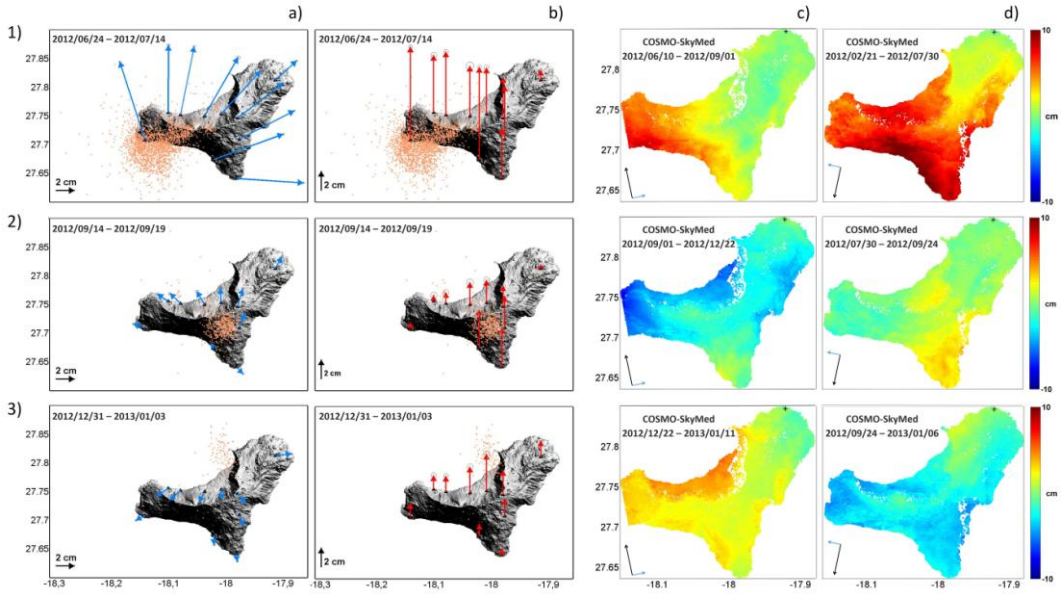

Fig. 4. El Hierro ground surface deformation maps for the post-eruption intrusive events: 1) 2012 June/July intrusion, 2) 2012 September intrusion, 3) 2013 January intrusion. Columns a) and b) show the horizontal (blue arrows) and vertical (red arrows) GPS displacements respectively, with 95% confidence ellipses, recorded by the cGPS stations for each intrusive event. Orange dots display the location of earthquakes in latitude and longitude. Columns c) and d) show the unwrapped interferograms in ascending and descending modes of the satellites respectively, spanning each intrusive episode. LOS displacements are positive toward the satellite and are given relative to a reference point in the north of the island, marked by an asterisk. Satellite flight and look direction are shown with black and blue-arrows respectively.

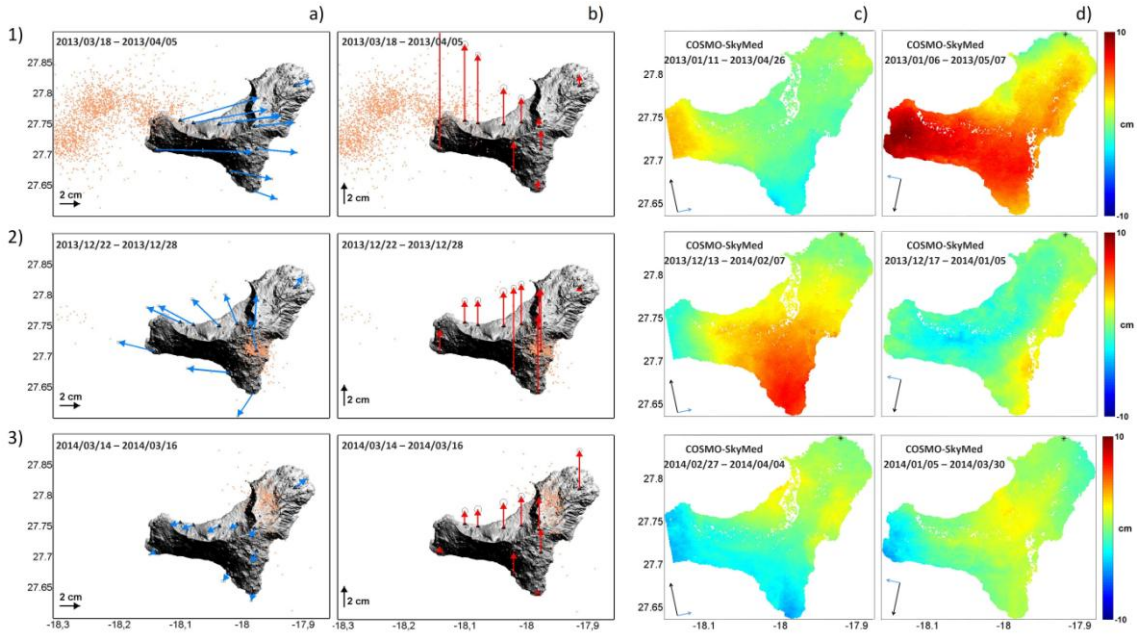

Fig. 5. El Hierro ground surface deformation maps for the post-eruption intrusive events: 1) 2013 March/April intrusion, 2) 2013 December intrusion, 3) 2014 March intrusion. Columns and symbols are the same as in Fig. 4.

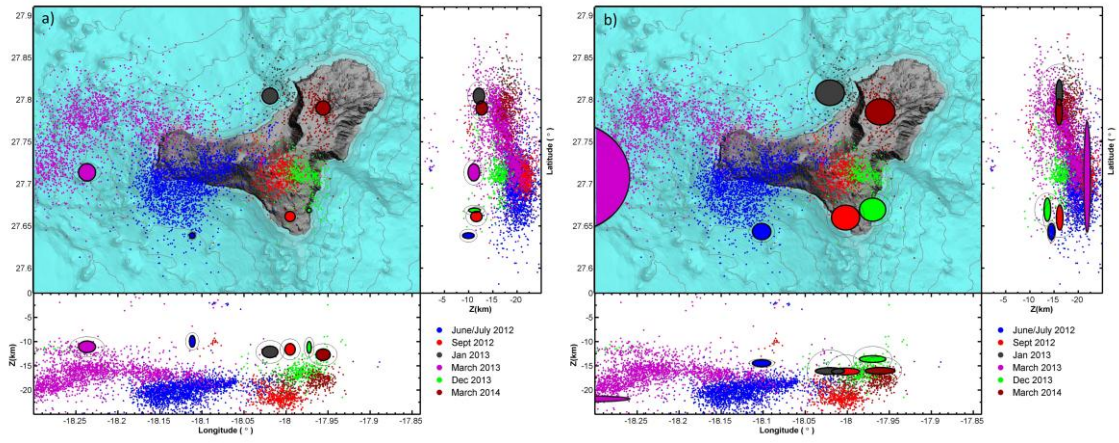

Fig. 6. a) Optimal spheroid and b) penny-shaped crack models obtained from the joint GPS and InSAR inversions for each of the 2012-2014 post-eruption magmatic intrusive events making no prior constraints on source parameters (position of the source, ΔV, radius, strike and dip were all free parameters).

Table 2. Source model parameters for each of the 2012-2014 post-eruption magmatic intrusions in El Hierro Island, obtained from jointly inversion of GPS and InSAR data.

2012 June/July intrusion												
Model	**Longitude (°)**	**Latitude (°)**	**Depth (km)**	**Volume (km^3)**	**Radius (km)**	**A (aspect ratio)**	**Length (km)**	**Width (km)**	**Dip (°)**	**Strike (°)**	**Opening (m)**	**RSS**
Sphere	-18.114 ± 0.001	27.638 ± 0.001	11.1 ± 0.1	0.122 ± 0.002								1.63
Spheroid	-18.112 ± 0.002	27.639 ± 0.002	9.9 ± 0.2	0.092 ± 0.006		0.3 ± 0.1			75 ± 4	360 ± 3		1.47
Sill	-18.102 ± 0.004	27.643 ± 0.003	14.5 ± 0.2	0.011 ± 0.001	1.10 ± 0.05							17.09
Dike	-18.209 ± 0.048	27.523 ± 0.055	2.4 ± 1.5	0.124 ± 0.525			1.0 ± 3.6	28.0 ± 10.7	-153 ± 30	-54 ± 22	4.4 ± 1.3	1.58
2012 September intrusion												
Sphere	-18.001 ± 0.002	27.660 ± 0.002	11.5 ± 0.4	0.027 ± 0.002								1.44
Spheroid	-17.995 ± 0.003	27.661 ± 0.002	11.6 ± 0.6	0.027 ± 0.002		0.5 ± 0.1			-57 ± 11	107 ± 16		1.41
Sill	-18.002 ± 0.003	27.660 ± 0.007	16.2 ± 2.7	0.030 ± 0.008	1.68 ± 0.23							1.55
Dike	-18.005 ± 0.006	27.651 ± 0.008	13.5 ± 2.0	0.022 ± 0.068			3.0 ± 2.9	1.3 ± 1.9	-156 ± 15	-74 ± 18	6.0 ± 3.6	1.47
2013 January intrusion												
Sphere	-18.020 ± 0.003	27.801 ± 0.003	11.8 ± 0.6	0.023 ± 0.002								1.40
Spheroid	-18.019 ± 0.003	27.804 ± 0.003	12.1 ± 0.7	0.025 ± 0.002		0.8 ± 0.1			9 ± 29	5 ± 120		1.40
Sill	-18.021 ± 0.006	27.808 ± 0.015	16.1 ± 3.6	0.028 ± 0.010	1.73 ± 0.42							1.43
Dike	-18.058 ± 0.018	27.788 ± 0.038	13.3 ± 3.8	0.026 ± 0.171			2.1 ± 2.6	16.8 ± 7.1	-173 ± 34	69 ± 26	0.8 ± 3.6	1.42
2013 March/April intrusion												
Sphere	-18.231 ± 0.003	27.712 ± 0.001	11.0 ± 0.2	0.124 ± 0.004								1.05
Spheroid	-18.237 ± 0.006	27.714 ± 0.001	11.1 ± 0.5	0.133 ± 0.014		0.8 ± 0.0			-28 ± 41	224 ± 65		1.04
Sill	-18.333 ± 0.000	27.708 ± 0.001	21.8 ± 0.1	9.770 ± 0.044	7.44 ± 0.01							3849
Dike	-18.369 ± 0.060	27.682 ± 0.017	1.7 ± 3.1	0.113 ± 0.285			6.1 ± 3.0	27.6 ± 10.7	-148 ± 20	-14 ± 9	0.7 ± 1.1	0.96
2013 December intrusion												
Sphere	-17.972 ± 0.001	27.668 ± 0.001	9.9 ± 0.2	0.041 ± 0.001								1.48
Spheroid	-17.973 ± 0.002	27.669 ± 0.001	11.2 ± 0.5	0.041 ± 0.005		0.2 ± 0.1			2 ± 5	345 ± 7		1.27
Sill	-17.970 ± 0.005	27.669 ± 0.004	13.6 ± 1.9	0.044 ± 0.013	1.57 ± 0.20							2.08
Dike	-17.934 ± 0.006	27.655 ± 0.004	7.6 ± 0.6	0.034 ± 0.055			1.2 ± 1.4	11.5 ± 2.1	-33 ± 11	24 ± 6	2.5 ± 0.6	1.35

2014 March intrusion												
Sphere	-17.959 ± 0.004	27.784 ± 0.003	12.3 ± 0.7	0.023 ± 0.002								0.63
Spheroid	-17.956 ± 0.004	27.790 ± 0.003	12.7 ± 0.7	0.028 ± 0.003		0.7 ± 0.1			-40 ± 9	130 ± 13		0.62
Sill	-17.961 ± 0.005	27.786 ± 0.006	16.0 ± 2.2	0.025 ± 0.006	1.77 ± 0.23							0.63
Dike	-18.039 ± 0.031	27.812 ± 0.015	14.8 ± 2.5	0.026 ± 0.081			2.3 ± 2.8	17.0 ± 5.7	-179 ± 21	22 ± 13	0.7 ± 1.0	0.62

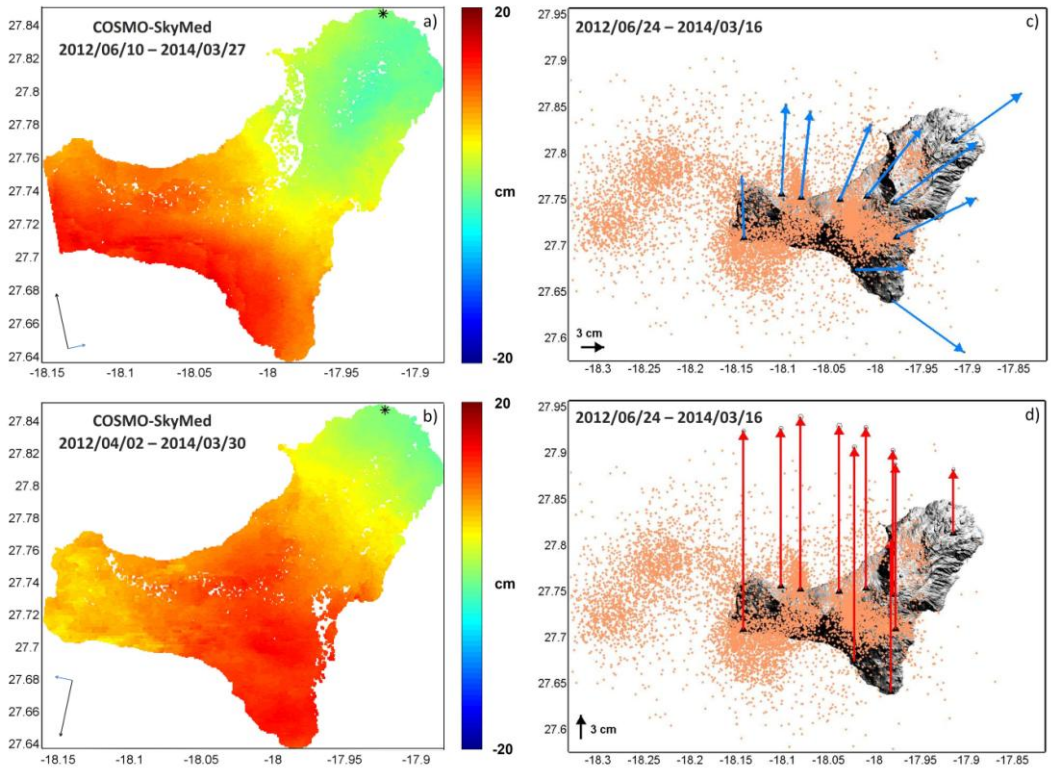

Fig. 7. June 2012 – March 2014 El Hierro ground surface displacement maps. a) Unwrapped CSK interferogram in ascending mode spanning 10 June 2012 to 27 March 2014. b) Unwrapped interferogram in descending mode spanning 2 April 2012 to 30 March 2014. LOS displacements are given relative to a reference point in the north of the island, marked by an asterisk. c) Horizontal GPS displacement (blue arrows) and d) vertical displacements (red arrows), with 95% confidence ellipses, from 24 June 2012 to 16 March 2014 recorded by the cGPS stations. Orange dots represent epicenters of earthquakes recorded during the entire time period.

5. Discussion

We have measured ground surface deformation in El Hierro Island spanning the time period 2012 to 2014 using a combination of InSAR and GPS geodetic techniques. The high spatial density of InSAR data in both ascending and descending modes and the continuous three-dimensional GPS measurements have allowed us to obtain a comprehensive overview of the ground displacement which occurred as a consequence of the post-eruption magmatic intrusions between 2012 and 2014. Elastic analytical modeling of the ground deformation using a MCMC approach has been employed to infer the volcanic sources responsible for the observed deformations. We have tested a point pressure spherical source, a spheroid, a penny-shaped crack and a rectangular dislocation model in an elastic, homogeneous, isotropic half-space, and inverted the GPS and InSAR datasets simultaneously to determine the optimal source parameters (location, geometry, volume/pressure change) that minimized the misfit between the observations and the models.

Our results indicate that six post-eruption intrusions have occurred in El Hierro Island between June 2012 and March 2014 revealed by intense seismic swarms and rapid surface displacements. Earthquake hypocenters combined with location and volume change estimates for each of the volcanic sources suggest that magmatic processes were responsible for these events. As a consequence of these events, the surface of the island has inflated more than 20 cm in the central-western part (up to 27 cm of vertical displacement has been recorded at cGPS station HI10) corresponding to a large accumulation of magma beneath the surface (~0.32-0.38 km^3) (Fig. 7).

It is reasonable to assume that these post-eruptive events are associated with episodes of magma supply coming from the mantle underneath El Hierro. A low-density layer with different rheology and properties is possibly capturing the magma on its way

to the surface (Taisne and Jaupart, 2009). We suggest that this discontinuity is the mantle/lower crust transition according to the depths of earthquakes and geodetic source models combined with the results of previous geophysical studies carried out in the Canary Islands (Banda et al., 1981; Bosshard and MacFarlane, 1970; Lodge et al., 2012; Ranero et al., 1995; Watts, 1994).

If the ascent of magma is impeded at the Mohorovičić (Moho) discontinuity, it may extend laterally, possibly forming a sill (Kavanagh et al., 2006). The location and migration of hypocenters, especially during the June-July 2012 and March-April 2013 intrusive events, suggest that these intrusions may be considered as evolving horizontal dikes or sill-like bodies. Multiple source locations of the geodetic data provide similar locations in latitude/longitude for the sphere, spheroid, dike, and penny-shaped crack models, whereby the spheroid model typically has the minimum RSS. However, the penny-shaped crack model, representing a sill-like body, also fits the data well in most of the intrusive episodes and is typically 3-5 km deeper, located near the top of the seismicity.

The large residuals for this source model for the two longest intrusive events may be due to the increased distance between the location of the source and the island, which was especially significant during the March/April 2013 event. Nonetheless, the strong agreement between the location of seismicity and the geodetic penny-shaped crack models for the magmatic intrusive events that occurred below the island and the location of the mantle/lower crust discontinuity at these depths suggest an ascent of magma from the mantle that stopped at ~14-16 km depth. Due to the inability of the magma to make its way to the surface, melt accumulates along this boundary.

Each of these post-eruption magmatic intrusions, with volume changes between ~0.02 and 0.13 km^3, occurred below the island in an area not previously affected by the

preceding intrusions. All the intrusions started beneath one of the three rifts of the island, and for two of the events, magma had enough pressure to migrate, always following a lateral path away from the center of the island, as revealed by seismicity and geodetic data.

Our results also confirm that despite the seismic energy released, the ground surface deformation and the associated volume source change, magmatic intrusive events do not always result in an eruption (Moran et al., 2011). The six magmatic post-eruption intrusions studied here have been more energetic that the intrusion recorded in July 2011 at El Hierro, which culminated in the 2011-2012 submarine eruption. The maximum uplift recorded in the island in the three months prior to the onset of the eruption was ~5 cm (López et al., 2012) with an estimated volume change of 0.04 km^3 of a spherical source located at a depth of ~9.5 km (González et al., 2013). During the December 2013 intrusion, the maximum vertical uplift was ~8 cm measured over only six days with an estimated volume change of 0.04 km^3 at ~10 km depth for a point pressure source.

Magmatic sill intrusions have occurred at other volcanoes. Without culminating in an eruption, the Three Sisters volcanic center, Oregon, showed approximately 14 cm of uplift between 1995 and 2001 associated with an intrusion of magma at ~6.5 km depth (Dzurisin et al., 2006; Wicks et al., 2002) and the Lazufre region, central Andes, exhibited large-scale uplift at a rate of about 3 cm/yr, between 1998 and 2002 modelled by an inflating sill (Pearse and Lundgren, 2013). Extensive magmatic intrusions were also observed in different areas beneath the Eyjafjallajökull volcano, Iceland, in 1994 and 1999 prior to the 2010 eruption (Pedersen and Sigmundsson, 2004; Pedersen and Sigmundsson, 2006).

The El Hierro intrusive events represent a clear example of several post-eruptive deep intrusions beneath an oceanic intraplate island which occurred on a time scale of months, after a period of quiescence of several hundred years. It is plausible that the 1793 seismic crisis reported in historical documents may have been another sequence of short-lived intrusive events, as the ones reported in this study.

However, modeling of surface displacements does not provide a unique solution for the source of the deformation. Model assumptions, simplifications, and data uncertainty complicate the interpretation (Lisowski, 2007). For example, the GPS network and InSAR images are limited by the size and geometry of the island. Most probably, these post-eruption intrusive events have produced ground deformation in the surface below the sea level that we have not been able to measure. Nonetheless, the inversion of the geodetic subaerial datasets has allowed us to estimate the volcanic sources responsible for such surface deformations, and their locations are in good agreement with the seismicity recorded during the same periods. Atmospheric noise is considered to be the largest contributor to error in our interferograms. Increasing the number of SAR acquisitions over the island will improve the signal to noise ratio, aiding deformation analysis and in turn improving the optimal source parameters of future intrusions. Furthermore, the analytical source models used to invert the ground deformation data are characterized by being flat Earth models that assume a simple pressure source in a homogeneous, isotropic, elastic half-space. Heterogeneities of the crust, in both lithology and temperature for example, affect the deformation signal observed in the surface (Masterlark et al., 2012); however this information is not available for use in this study. Despite their limitations, the elastic half-space models are widely used primarily because of the simplicity of the equations, the good approximation of the sources obtained, and the rapid processing times, making these

models useful for near-real time volcano monitoring (Lisowski, 2007). In this study, the modeled depth range and location of the magma sources are considered reasonable and in broad agreement with the spatial distribution of the relocated earthquakes, taking into consideration also their location errors (Díaz-Moreno et al., 2015).

More realistic Earth models accounting for curvature, topography, vertical layering, lateral heterogeneities, and time-varying material properties can be employed where appropriate. However, additional information about the magma rheology, mechanical properties and lateral heterogeneities of the crust would be necessary to employ such models at El Hierro.

Understanding the evolution of magmatic intrusions in the Earth's crust is critical for accurate interpretation of geophysical and geochemical monitoring data and, ultimately, eruption forecasting and mitigation of the associated volcanic risk. Geodetic and seismic observations are essential to identify the initiation of new intrusions, their location, and magma supply rates, the details of which may assist in determining whether future intrusions at El Hierro are likely to trigger an eruption.

This is the first study to analyze the 2012-2014 post-eruption magmatic intrusions from geodetic observations, using GPS and InSAR data. These events provided a remarkable opportunity to study the magmatic plumbing system of El Hierro, a volcanic island exhibiting short-phases of monogenetic volcanism with significantly longer periods of quiescence. Our results corroborate the hypothesis of magma stagnation at the crustal-mantle discontinuity and the formation of a network of magma reservoirs distributed beneath the island (Albert et al., 2016; Stroncik et al., 2009). The recorded activity improves our understanding of how an oceanic intraplate volcanic island grows through repeated magmatic intrusions; well documented by seismic, GPS and InSAR observations in the case of the El Hierro Island.

6. Conclusion

Six post-eruption magmatic intrusions occurred beneath El Hierro Island from June 2012 to March 2014. Despite these intrusive events being more energetic and producing larger amounts of surface deformation than the first pre-eruptive intrusion (detected on July 2011 after more than 200 years of quiescence) they did not culminate in an eruption. The first post-eruptive intrusion occurred only three months after the end of the submarine eruption, and the last magmatic intrusion was detected two years later. These intrusive events have been separated by only a few months and have lasted between 3 and ~27 days. We interpret these intrusive events as episodic magma trapping at the Moho discontinuity at ~14-16 km depth, following deep magma migration from the mantle. We suggest these intrusions are sill-like bodies with volume changes between 0.02 and 0.13 km^3 that migrated laterally during the 2012 June/July and 2013 March/April events. These new batches of magma, which have accumulated beneath El Hierro, (~0.32-0.38 km^3 of melt) have contributed to the growth of the island with more than 20 cm of outward displacement in the central and western part in less than two years. Further work is required to ascertain why some intrusions culminate in an eruption while others, even more energetic, do not. These events present a rare opportunity to study the plumbing system of a volcanic intraplate island and how this evolves over time.

Acknowledgements

This research has been supported by IGN, a grant from Iceland, Liechtenstein and Norway through the EEA Financial Mechanism, Operated by University Complutense de Madrid, and CGL2014-58821-C2-1-R MINECO research project, and European Community's Seventh Framework Programme grant no. 308377 (Project FUTUREVOLC). RADARSAT-2 and COSMO-SkyMed images were provided by the European Space Agency under CAT1 29252 and 31045 projects respectively.

We wish to thank the IGN group for the deployment and maintenance of the volcano monitoring network on El Hierro Island. We appreciate the constructive comments by V. Villasante-Marcos, and thank R. Abella, for sharing Matlab scripts that were used to create some of the figures, and M. Fernández-de Villalta, for providing a DEM-Bathymetry image of El Hierro.. We are grateful to C. López for her support with this collaboration. We also thank M. Poland, P. Lundgren, and an anonymous reviewer for their constructive review of the manuscript.

References

Acosta, J., Uchupi, E., Smith, D., Munoz, A., Herranz, P., Palomo, C., Llanes, P., Ballesteros, M. and Grp, Z.E.E.W., 2003. Comparison of volcanic rifts on La Palma and El Hierro, Canary Islands and the Island of Hawaii. Marine Geophysical Researches, 24(1-2): 59-90.

Albert, H., Costa, F. and Martí, J., 2016. Years to weeks of seismic unrest and magmatic intrusions precede monogenetic eruptions. Geology.

Banda, E., Danobeitia, J.J., Surinach, E. and Ansorge, J., 1981. Features of crustal structure under the Canary Islands. Earth and Planetary Science Letters, 55(1): 11-24.

Battaglia, M., Troise, C., Obrizzo, F., Pingue, F. and De Natale, G., 2006. Evidence for fluid migration as the source of deformation at Campi Flegrei caldera (Italy). Geophysical Research Letters, 33(1): 4.

Becerril, L., Galindo, I., Marti, J. and Gudmundsson, A., 2015. Three-armed rifts or masked radial pattern of eruptive fissures? The intriguing case of El Hierro volcano (Canary Islands). Tectonophysics, 647: 33-47.

Bekaert, D.P.S., Hooper, A. and Wright, T.J., 2015a. A spatially variable power law tropospheric correction technique for InSAR data. Journal of Geophysical Research-Solid Earth, 120(2): 1345-1356.

Bekaert, D.P.S., Walters, R.J., Wright, T.J., Hooper, A.J. and Parker, D.J., 2015b. Statistical comparison of InSAR tropospheric correction techniques. Remote Sensing of Environment, 170: 40-47.

Biggs, J., Anthony, E.Y. and Ebinger, C.J., 2009. Multiple inflation and deflation events at Kenyan volcanoes, East African Rift. Geology, 37(11): 979-982.

Blanco-Montenegro, I., Nicolosi, I., Pignatelli, A. and Chiappini, M., 2008. Magnetic imaging of the feeding system of oceanic volcanic islands: El Hierro (Canary Islands). Geophysical Journal International, 173(1): 339-350.

Bosshard, E. and MacFarlane, D.J., 1970. Crustal structure of western Canary-Islands from seismic refraction and gravity data. Journal of Geophysical Research, 75(26): 4901-&.

Carracedo, J.C., 1994. The Canary Islands: an example of structural control on the growth of large oceanic-island volcanoes. Journal of Volcanology and Geothermal Research, 60(3): 225-241.

Carracedo, J.C., Day, S.J., Guillou, H. and Torrado, F.J.P., 1999. Giant Quaternary landslides in the evolution of La Palma and El Hierro, Canary Islands. Journal of Volcanology and Geothermal Research, 94(1-4): 169-190.

Carracedo, J.C., Pérez Torrado, F., Rodríguez González, A., Soler, V., Turiel Fernández, J.L., Troll, V.R. and Wiesmaier, S., 2012. The 2011 submarine volcanic eruption in El Hierro (Canary Islands). Geology Today, 28(2): 53--58.

Carracedo, J.C., Rodríguez Badiola, E., Guillou, H., de la Nuez, J. and Pérez Torrado, F.J., 2001. Geology and volcanology of La Palma and El Hierro, Western Canaries. 57(5-6): 175–273.

Chaussard, E. and Amelung, F., 2012. Precursory inflation of shallow magma reservoirs at west Sunda volcanoes detected by InSAR. Geophysical Research Letters, 39: 6.

Dach, R., Lutz, S., Walser, P. and Fridez, P. (Editors), 2015. Bernese GNSS Software Version 5.2. User manual. Astronomical Institute, University of Bern, Bern Open Publishing.

Darias y Padrón, D.V., 1929. Noticias generales históricas sobre la isla de El Hierro. Imprenta Curbelo, La Laguna de Tenerife, pp. 497,.

Decriem, J., Arnadottir, T., Hooper, A., Geirsson, H., Sigmundsson, F., Keiding, M., Ofeigsson, B.G., Hreinsdottir, S., Einarsson, P., LaFemina, P. and Bennett, R.A., 2010. The 2008 May 29 earthquake doublet in SW Iceland. Geophysical Journal International, 181(2): 1128-1146.

del Fresno, C., Domínguez Cerdeña, I., Cesca, S. and Buforn, E., 2015. The 8 October 2011 Earthquake at El Hierro (M-w 4.0): Focal Mechanisms of the Mainshock and Its Foreshocks. Bulletin of the Seismological Society of America, 105(1): 330-340.

Del Moro, S., Di Roberto, A., Meletlidis, S., Pompilio, M., Bertagnini, A., Agostini, S., Ridolfi, F. and Renzulli, A., 2015. Xenopumice erupted on 15 October 2011 offshore of El Hierro (Canary Islands): a subvolcanic snapshot of magmatic, hydrothermal and pyrometamorphic processes. Bulletin of Volcanology, 77(6): 19.

Domínguez Cerdeña, I., del Fresno, C. and Moreno, A.G., 2014. Seismicity Patterns Prior to the 2011 El Hierro Eruption. Bulletin of the Seismological Society of America, 104(1): 567-575.

Dzurisin, D., Lisowski, M., Wicks, C.W., Poland, M.P. and Endo, E.T., 2006. Geodetic observations and modeling of magmatic inflation at the Three Sisters volcanic center, central Oregon Cascade Range, USA. Journal of Volcanology and Geothermal Research, 150(1-3): 35-54.

Díaz-Moreno, A., Ibanez, J.M., De Angelis, S., Garcia-Yeguas, A., Prudencio, J., Morales, J., Tuve, T. and Garcia, L., 2015. Seismic hydraulic fracture migration originated by successive deep magma pulses: The 2011-2013 seismic series associated to the volcanic activity of El Hierro Island. Journal of Geophysical Research-Solid Earth, 120(11): 7749-7770.

Fialko, Y., Khazan, Y. and Simons, M., 2001. Deformation due to a pressurized horizontal circular crack in an elastic half-space, with applications to volcano geodesy. Geophysical Journal International, 146(1): 181-190.

García, A., Fernández-Ros, A., Berrocoso, M., Marrero, J.M., Prates, G., De la Cruz-Reyna, S. and Ortiz, R., 2014. Magma displacements under insular volcanic fields, applications to eruption forecasting: El Hierro, Canary Islands, 2011-2013. Geophysical Journal International, 197(1): 322-334.

Gee, M.J.R., Masson, D.G., Watts, A.B. and Mitchell, N.C., 2001a. Offshore continuation of volcanic rift zones, El Hierro, Canary Islands. Journal of Volcanology and Geothermal Research, 105(1-2): 107-119.

Gee, M.J.R., Watts, A.B., Masson, D.G. and Mitchell, N.C., 2001b. Landslides and the evolution of El Hierro in the Canary Islands. Marine Geology, 177(3-4): 271-293.

Goldstein, R.M., Zebker, H.A. and Werner, C.L., 1988. Satellite radar interferometry - Two-dimensional phase unwrapping. Radio Science, 23(4): 713-720.

Gonzalez, P.J., Tiampo, K.F., Camacho, A.G. and Fernandez, J., 2010. Shallow flank deformation at Cumbre Vieja volcano (Canary Islands): Implications on the stability of steep-sided volcano flanks at oceanic islands. Earth and Planetary Science Letters, 297(3-4): 545-557.

González, P.J., Samsonov, S.V., Pepe, S., Tiampo, K.F., Tizzani, P., Casu, F., Fernandez, J., Camacho, A.G. and Sansosti, E., 2013. Magma storage and migration associated with the 2011-2012 El Hierro eruption: Implications for crustal magmatic systems at oceanic island volcanoes. Journal of Geophysical Research-Solid Earth, 118(8): 4361-4377.

Guillou, H., Carracedo, J.C., Torrado, F.P. and Badiola, E.R., 1996. K-Ar ages and magnetic stratigraphy of a hotspot-induced, fast grown oceanic island: El Hierro, Canary Islands. Journal of Volcanology and Geothermal Research, 73(1-2): 141-155.

Hooper, A., 2008. A multi-temporal InSAR method incorporating both persistent scatterer and small baseline approaches. Geophysical Research Letters, 35(16): 5.

Hooper, A., 2010. A Statistical-Cost Approach to Unwrapping the Phase of InSAR Time Series. *Proceedings 2009 FRINGE Workshop*, Frascati, 2010. .

Hooper, A., Bekaert, D., Spaans, K. and Arikan, M., 2012. Recent advances in SAR interferometry time series analysis for measuring crustal deformation. Tectonophysics, 514: 1-13.

Hooper, A., Segall, P. and Zebker, H., 2007. Persistent scatterer interferometric synthetic aperture radar for crustal deformation analysis, with application to Volcan Alcedo, Galapagos. Journal of Geophysical Research-Solid Earth, 112(B7): 21.

Hooper, A., Zebker, H., Segall, P. and Kampes, B., 2004. A new method for measuring deformation on volcanoes and other natural terrains using InSAR persistent scatterers. Geophysical research letters, 31(23).

Ibáñez, J.M., De Angelis, S., Díaz-Moreno, A., Hernández, P., Alguacil, G., Posadas, A. and Pérez, N., 2012. Insights into the 2011-2012 submarine eruption off the coast of El Hierro (Canary Islands, Spain) from statistical analyses of earthquake activity. Geophysical Journal International, 191(2): 659-670.

Kampes, B.M., Hanssen, R.F. and Perski, Z., 2003. Radar interferometry with public domain tools, Proceedings of FRINGE, pp. 1-5.

Kavanagh, J.L., Menand, T. and Sparks, R.S.J., 2006. An experimental investigation of sill formation and propagation in layered elastic media. Earth and Planetary Science Letters, 245(3-4): 799-813.

Klügel, A., Longpré, M.A., García-Cañada, L. and Stix, J., 2015. Deep intrusions, lateral magma transport and related uplift at ocean island volcanoes. Earth and Planetary Science Letters, 431: 140 - 149.

Lisowski, M., 2007. Analytical volcano deformation source models, Volcano Deformation. Springer, pp. 279-304.

Lodge, A., Nippress, S.E.J., Rietbrock, A., Garcia-Yeguas, A. and Ibanez, J.M., 2012. Evidence for magmatic underplating and partial melt beneath the Canary Islands derived using teleseismic receiver functions. Physics of the Earth and Planetary Interiors, 212: 44-54.

Longpré, M.A., Chadwick, J.P., Wijbrans, J. and Iping, R., 2011. Age of the El Golfo debris avalanche, El Hierro (Canary Islands): New constraints from laser and furnace Ar-40/Ar-39 dating. Journal of Volcanology and Geothermal Research, 203(1-2): 76-80.

Longpré, M.A., Klügel, A., Diehl, A. and Stix, J., 2014. Mixing in mantle magma reservoirs prior to and during the 2011-2012 eruption at El Hierro, Canary Islands. Geology, 42(4): 315-318.

Lu, Z., Dzurisin, D., Biggs, J., Wicks, C. and McNutt, S., 2010. Ground surface deformation patterns, magma supply, and magma storage at Okmok volcano, Alaska, from InSAR analysis: 1. Intereruption deformation, 1997-2008. Journal of Geophysical Research-Solid Earth, 115: 14.

López, C., Blanco, M.J., Abella, R., Brenes, B., Cabrera Rodríguez, V.M., Casas, B., Domínguez Cerdeña, I., Felpeto, A., Fernández de Villalta, M., del Fresno, C., García, O., García-Arias, M.J., García-Cañada, L., Gomis Moreno, A., González-Alonso, E., Guzmán Pérez, J., Iribarren, I., López-Díaz, R., Luengo-Oroz, N., Meletlidis, S., Moreno, M., Moure, D., Pereda de Pablo, J., Rodero, C., Romero, E., Sainz-Maza, S., Sentre Domingo, M.A., Torres, P.A., Trigo, P. and Villasante-Marcos, V., 2012. Monitoring the volcanic unrest of El Hierro (Canary Islands) before the onset of the 2011-2012 submarine eruption. Geophysical Research Letters, 39: 7.

López, C., Martí, J., Abella, R. and Tarraga, M., 2014. Applying Fractal Dimensions and Energy-Budget Analysis to Characterize Fracturing Processes During Magma Migration and Eruption: 2011-2012 El Hierro (Canary Islands) Submarine Eruption. Surveys in Geophysics, 35(4): 1023-1044.

Martí, J., Castro, A., Rodríguez, C., Costa, F., Carrasquilla, S., Pedreira, R. and Bolos, X., 2013a. Correlation of Magma Evolution and Geophysical Monitoring during the 2011-2012 El Hierro (Canary Islands) Submarine Eruption. Journal of Petrology, 54(7): 1349-1373.

Martí, J., Pinel, V., López, C., Geyer, A., Abella, R., Tárraga, M., Blanco, M.J., Castro, A. and Rodríguez, C., 2013b. Causes and mechanisms of the 2011-2012 El Hierro (Canary Islands) submarine eruption. Journal of Geophysical Research-Solid Earth, 118(3): 823-839.

Masson, D.G., 1996. Catastrophic collapse of the volcanic island of Hierro 15 ka ago and the history of landslides in the Canary Islands. Geology, 24(3): 231-234.

Masson, D.G., Watts, A.B., Gee, M.J.R., Urgeles, R., Mitchell, N.C., Le Bas, T.P. and Canals, M., 2002. Slope failures on the flanks of the western Canary Islands. Earth-Science Reviews, 57(1-2): 1-35.

Massonnet, D. and Feigl, K.L., 1995. Discrimination of geophysical phenomena in satellite radar interferograms. Geophysical Research Letters, 22(12): 1537-1540.

Massonnet, D. and Feigl, K.L., 1998. Radar interferometry and its application to changes in the earth's surface. Reviews of Geophysics, 36(4): 441-500.

Massonnet, D., Rossi, M., Carmona, C., Adragna, F., Peltzer, G., Feigl, K. and Rabaute, T., 1993. The displacement field of the Landers earthquake mapped by Radar Interferometry. Nature, 364(6433): 138-142.

Masterlark, T., Feigl, K.L., Haney, M., Stone, J., Thurber, C. and Ronchin, E., 2012. Nonlinear estimation of geometric parameters in FEMs of volcano deformation: Integrating tomography models and geodetic data for Okmok volcano, Alaska. Journal of Geophysical Research-Solid Earth, 117: 17.

Meletlidis, S., Di Roberto, A., Cerdena, I.D., Pompilio, M., Garcia-Canada, L., Bertagnini, A., Benito-Saz, M.A., Del Carlo, P. and Aparicio, S.S.M., 2015. New insight into the 2011-2012 unrest and eruption of El Hierro Island (Canary Islands) based on integrated geophysical, geodetical and petrological data. Annals of Geophysics, 58(5): 20.

Meletlidis, S., Di Roberto, A., Pompilio, M., Bertagnini, A., Iribarren, I., Felpeto, A., Torres, P.A. and D'Oriano, C., 2012. Xenopumices from the 2011-2012 submarine eruption of El Hierro (Canary Islands, Spain): Constraints on the plumbing system and magma ascent. Geophysical Research Letters, 39: 6.

Melián, G., Hernández, P.A., Padrón, E., Pérez, N.M., Barrancos, J., Padilla, G., Dionis, S., Rodríguez, F., Calvo, D. and Nolasco, D., 2014. Spatial and temporal variations of diffuse CO2 degassing at El Hierro volcanic system: Relation to the 2011-2012 submarine eruption. Journal of Geophysical Research-Solid Earth, 119(9): 6976-6991.

Mogi, K., 1958. Relations between the eruptions of various volcanoes and the deformations of the ground surfaces around them. Bull. Earthq. Res. Inst. Univ. Tokyo, 36: 99–134.

Moran, S.C., Newhall, C. and Roman, D.C., 2011. Failed magmatic eruptions: late-stage cessation of magma ascent. Bulletin of Volcanology, 73(2): 115-122.

Mosegaard, K. and Tarantola, A., 1995. Monte Carlo sampling of solutions to inverse problems. Journal of Geophysical Research-Solid Earth, 100(B7): 12431-12447.

Münn, S., Walter, T.R. and Klügel, A., 2006. Gravitational spreading controls rift zones and flank instability on El Hierro, Canary Islands. Geological Magazine, 143(3): 257-268.

Nishimura, T., Ozawa, S., Murakami, M., Sagiya, T., Tada, T., Kaidzu, M. and Ukawa, M., 2001. Crustal Deformation caused by magma migration in the northern Izu Islands, Japan. Geophysical Research Letters, 28(19): 3745-3748.

Okada, Y., 1985. Surface deformation due to shear and tensile faults in a half-space. Bulletin of the Seismological Society of America, 75(4): 1135-1154.

Okada, Y., 1992. Internal deformation due to shear and tensile faults in a half-space. Bulletin of the Seismological Society of America, 82(2): 1018-1040.

Padilla, G.D., Hernandez, P.A., Padron, E., Barrancos, J., Perez, N.M., Melian, G., Nolasco, D., Dionis, S., Rodriguez, F., Calvo, D. and Hernandez, I., 2013. Soil gas radon emissions and volcanic activity at El Hierro (Canary Islands): The 2011-2012 submarine eruption. Geochemistry Geophysics Geosystems, 14(2): 432-447.

Padron, E., Perez, N.M., Hernandez, P.A., Sumino, H., Melian, G.V., Barrancos, J., Nolasco, D., Padilla, G., Dionis, S., Rodriguez, F., Hernandez, I., Calvo, D., Peraza, M.D. and Nagao, K., 2013. Diffusive helium emissions as a precursory sign of volcanic unrest. Geology, 41(5): 539-542.

Parks, M.M., Biggs, J., Mather, T.A., Pyle, D.M., Amelung, F., Monsalve, M.L. and Medina, L.N., 2011. Co-eruptive subsidence at Galeras identified during an InSAR survey of Colombian volcanoes (2006-2009). Journal of Volcanology and Geothermal Research, 202(3-4): 228-240.

Pearse, J. and Lundgren, P., 2013. Source model of deformation at Lazufre volcanic center, central Andes, constrained by InSAR time series. Geophysical Research Letters, 40(6): 1059-1064.

Pedersen, R. and Sigmundsson, F., 2004. InSAR based sill model links spatially offset areas of deformation and seismicity for the 1994 unrest episode at Eyjafjallajokull volcano, Iceland. Geophysical Research Letters, 31(14).

Pedersen, R. and Sigmundsson, F., 2006. Temporal development of the 1999 intrusive episode in the Eyjafjallajokull volcano, Iceland, derived from InSAR images. Bulletin of Volcanology, 68(4): 377-393.

Pinel, V., Poland, M.P. and Hooper, A., 2014. Volcanology: Lessons learned from Synthetic Aperture Radar imagery. Journal of Volcanology and Geothermal Research, 289: 81-113.

Pritchard, M.E. and Simons, M., 2004. An InSAR-based survey of volcanic deformation in the central Andes. Geochemistry Geophysics Geosystems, 5: 42.

Pérez, N.M., Padilla, G.D., Padron, E., Hernandez, P.A., Melian, G.V., Barrancos, J., Dionis, S., Nolasco, D., Rodriguez, F., Calvo, D. and Hernandez, I., 2012. Precursory diffuse CO2 and H2S emission signatures of the 2011-2012 El Hierro submarine eruption, Canary Islands. Geophysical Research Letters, 39: 5.

Ranero, C.R., Torne, M. and Banda, E., 1995. Gravity and multichannel seismic reflection constraints on the lithospheric structure of the Canary Swell. Marine Geophysical Researches, 17(6): 519-534.

Rivera, J., Lastras, G., Canals, M., Acosta, J., Arrese, B., Hermida, N., Micallef, A., Tello, O. and Amblas, D., 2013. Construction of an oceanic island: Insights from the El Hierro (Canary Islands) 2011-2012 submarine volcanic eruption. Geology, 41(3): 355-358.

Romero Ruíz, C., 1990. Las manifestaciones volcánicas históricas del Archipiélago Canario. Universidad de La Laguna, Tenerife, Spain.

Sainz-Maza Aparicio, S., Arnoso Sampedro, J., Gonzalez Montesinos, F. and Marti Molist, J., 2014. Volcanic signatures in time gravity variations during the volcanic unrest on El Hierro (Canary Islands). Journal of Geophysical Research-Solid Earth, 119(6): 5033-5051.

Sigmarsson, O., Laporte, D., Carpentier, M., Devouard, B., Devidal, J.L. and Marti, J., 2013. Formation of U-depleted rhyolite from a basanite at El Hierro, Canary Islands. Contributions to Mineralogy and Petrology, 165(3): 601-622.

Sigmundsson, F., Hooper, A., Hreinsdottir, S., Vogfjord, K.S., Ofeigsson, B.G., Heimisson, E.R., Dumont, S., Parks, M., Spaans, K., Gudmundsson, G.B., Drouin, V., Arnadottir, T., Jonsdottir, K., Gudmundsson, M.T., Hognadottir, T., Fridriksdottir, H.M., Hensch, M., Einarsson, P., Magnusson, E., Samsonov, S., Brandsdottir, B., White, R.S., Agustsdottir, T., Greenfield, T., Green, R.G., Hjartardottir, A.R., Pedersen, R., Bennett, R.A., Geirsson, H., La Femina, P.C., Bjornsson, H., Palsson, F., Sturkell, E., Bean, C.J., Mollhoff, M., Braiden, A.K. and Eibl, E.P.S., 2015. Segmented lateral dyke growth in a rifting event at Bardarbunga volcanic system, Iceland. Nature, 517(7533): 191-U158.

Sigmundsson, F., Hreinsdottir, S., Hooper, A., Arnadottir, T., Pedersen, R., Roberts, M.J., Oskarsson, N., Auriac, A., Decriem, J., Einarsson, P., Geirsson, H., Hensch, M., Ofeigsson, B.G., Sturkell, E., Sveinbjornsson, H. and Feigl, K.L., 2010. Intrusion triggering of the 2010 Eyjafjallajokull explosive eruption. Nature, 468(7322): 426-U253.

Solaro, G., Acocella, V., Pepe, S., Ruch, J., Neri, M. and Sansosti, E., 2010. Anatomy of an unstable volcano from InSAR: Multiple processes affecting flank instability at Mt. Etna, 1994-2008. Journal of Geophysical Research-Solid Earth, 115: 21.

Stroncik, N.A., Klügel, A. and Hansteen, T.H., 2009. The magmatic plumbing system beneath El Hierro (Canary Islands): constraints from phenocrysts and naturally quenched basaltic glasses in submarine rocks. Contributions to Mineralogy and Petrology, 157(5): 593-607.

Taisne, B. and Jaupart, C., 2009. Dike propagation through layered rocks. Journal of Geophysical Research-Solid Earth, 114: 18.

Telesca, L., Lovallo, M., López, C. and Marti Molist, J., 2016. Multiparametric statistical investigation of seismicity occurred at El Hierro (Canary Islands) from 2011 to 2014. Tectonophysics, 672–673: 121 - 128.

Troll, V.R., Klügel, A., Longpré, M.A., Burchardt, S., Deegan, F.M., Carracedo, J.C., Wiesmaier, S., Kueppers, U., Dahren, B., Blythe, L.S., Hansteen, T.H., Freda, C., Budd, D.A., Jolis, E.M., Jonsson, E., Meade, F.C., Harris, C., Berg, S.E., Mancini, L., Polacci, M. and Pedroza, K., 2012. Floating stones off El Hierro, Canary Islands: xenoliths of pre-island sedimentary origin in the early products of the October 2011 eruption. Solid Earth, 3(1): 97-110.

Urgeles, R., Canals, M., Baraza, J., Alonso, B. and Masson, D., 1997. The most recent megalandslides of the Canary Islands: El Golfo debris avalanche and Canary debris flow, west El Hierro island. Journal of Geophysical Research-Solid Earth, 102(B9): 20305-20323.

Villasante-Marcos, V. and Pavon-Carrasco, F.J., 2014. Palaeomagnetic constraints on the age of Lomo Negro volcanic eruption (El Hierro, Canary Islands). Geophysical Journal International, 199(3): 1497-1514.

Watson, I.M., Oppenheimer, C., Voight, B., Francis, P., Clarke, A., Stix, J., Miller, A., Pyle, D.M., Burton, M.R., Young, S.R., Norton, G., Loughlin, S., Darroux, B. and Staff, M.V.O., 2000. The relationship between degassing and ground deformation at Soufriere Hills Volcano, Montserrat. Journal of Volcanology and Geothermal Research, 98(1-4): 117-126.

Watts, A.B., 1994. Crustal structure, gravity-anomalies and flexure of the lithosphere in the vicinity of the Canary-Islands. Geophysical Journal International, 119(2): 648-666.

Watts, A.B., Peirce, C., Collier, J., Dalwood, R., Canales, J.P. and Henstock, T.J., 1997. A seismic study of lithospheric flexure in the vicinity of Tenerife, Canary Islands. Earth and Planetary Science Letters, 146(3-4): 431-447.

Wicks, C.W., Dzurisin, D., Ingebritsen, S., Thatcher, W., Lu, Z. and Iverson, J., 2002. Magmatic activity beneath the quiescent Three Sisters volcanic center, central Oregon Cascade Range, USA. Geophysical Research Letters, 29(7): 4.

Yang, X.M., Davis, P.M. and Dieterich, J.H., 1988. Deformation from inflation of a dipping finite prolate spheroid in an elastic half-space as a model for volcanic stressing. Journal of Geophysical Research-Solid Earth and Planets, 93(B5): 4249-4257.

Zebker, H.A., Rosen, P.A., Goldstein, R.M., Gabriel, A. and Werner, C.L., 1994. On the derivation of coseismic displacement-field using differential radar interferometry - The Landers earthquake. Journal of Geophysical Research-Solid Earth, 99(B10): 19617-19634.

Highlights

- Six deep magmatic intrusions at El Hierro Island following the 2011-2012 eruption.
- GPS and InSAR data reveal up to 27 cm of uplift from June 2012 to March 2014.
- Events likely related to pulses of magma coming from the mantle, trapped at the Moho.
- A total of 0.32–0.38 km^3 of melt has been accumulated beneath the island.
- Deformation modeling and seismicity suggests sill-like bodies intruded at depths of ~14-16 km.